Spring 2021

Implementation of a Constraint and Configuration Interaction Methodology Into Density Functional Tight Binding

Gunnar J. Carlson
Western Washington University, carlsog4@wwu.edu

IMPLEMENTATION OF A CONSTRAINT AND CONFIGURATION INTERACTION METHODOLOGY INTO DENSITY FUNCTIONAL TIGHT BINDING

By

GUNNAR JAY CARLSON

Accepted in Partial Completion
of the Requirements for the Degree
Master of Science

ADVISORY COMMITTEE

Dr. Tim Kowalczyk, Chair

Dr. Robert Berger

Dr. John Gilbertson

WESTERN WASHINGTON UNIVERSITY
Graduate School

Dr. David L. Patrick, Dean

MASTER'S THESIS

In presenting this thesis in partial fulfillment of the requirements for a master's degree at Western Washington University, I grant to Western Washington University the non-exclusive royalty-free right to archive, reproduce, distribute, and display the thesis in any and all forms, including electronic format, via any digital library mechanisms maintained by WWU.

I represent and warrant this is my original work, and does not infringe or violate any rights of others. I warrant that I have obtained written permissions from the owner of any third party copyrighted material included in these files.

I acknowledge that I retain ownership rights to the copyright of this work, including but not limited to the right to use all or part of this work in future works, such as articles or books.

Library users are granted permission for individual, research and non-commercial reproduction of this work for educational purposes only. Any further digital posting of this document requires specific permission from the author.

Any copying or publication of this thesis for commercial purposes, or for financial gain, is not allowed without my written permission.

Gunnar Jay Carlson

Spring 2021

IMPLEMENTATION OF A CONSTRAINT AND CONFIGURATION INTERACTION METHODOLOGY INTO DENSITY FUNCTIONAL TIGHT BINDING

A Thesis
Presented to
The Faculty of
Western Washington University

In Partial Fulfillment
Of the Requirements for the Degree
Master of Science

By
Gunnar Jay Carlson
Spring 2021

ABSTRACT

This research aims to implement a charge constraint in conjunction with a small configuration interaction scheme into a density-functional tight-binding (DFTB) method within the DFTB+ quantum mechanical software package. This method aims to model the electron transfer rate of chemical systems by calculating the electronic couplings between two constrained states more efficiently. Electronic couplings are directly proportional to electron transfer, making them important parameters to efficiently compute the optimal minimum or maximum of an electron transfer rate, for example, when screening chemical systems based on their ability as a conductor. Other methods such as constrained density-functional theory followed by a small configuration interaction scheme (CDFT-CI) developed by Wu and Van Voorhis can calculate electronic couplings. Still, as the complexity of chemical systems increases, the computational cost of CDFT-CI becomes intractable.

Using CDFT-CI as a starting point, we can develop a constrained density-functional tight-binding followed by a small configuration interaction scheme (CDFTB-CI) to lower computational costs compared to CDFT-CI. The strategies to implement a CDFTB-CI option into DFTB+ utilize built-in features of DFTB+ while being as non-intrusive as possible. This process introduces a constraint option in DFTB+ with the capabilities of calculating constrained energies of constrained states of simple molecules, such as a set of simple homogeneous and heterogeneous dimers. This set of simple molecules can be used as case studies with the implications of finding the best practices for CDFTB.

ACKNOWLEDGMENT

I want to thank the National Science Foundation for supporting this project under the award DMR-1848067. A huge thanks to Dr. Kowalczyk, who has mentored me through the last four years of my education at Western Washington University. Lastly, I want to thank my parents, who encouraged and counseled me through the highs and lows of this challenging but rewarding and fulfilling journey to acquire my master's.

TABLE OF CONTENTS

LIST OF TABLES

LIST OF FIGURES

Chapter One

Introduction

1.1 Electronic Couplings

The theoretical interest in electron transfer reactions over recent decades has led to continued refinement in numerical estimates of electron transfer parameters.[1–3] The common experimental electron transfer processes are intramolecular between two charged sites including flexible biomolecules and solvent molecules.[4] The increasing complexity of these chemical systems has driven up computational costs, necessitating the more efficient computation of computing these electron transfer parameters more efficiently. As seen in equation(1.1),[5] there are three electron transfer parameters that describe the electron transfer adequately.

$$k_{et} = \frac{2\pi}{\hbar}\langle|H_{ab}|^2\rangle(4\pi k_B T\lambda)^{-1/2}\exp\left[-\frac{(\lambda+\triangle G^o)^2}{4k_B T\lambda}\right] \tag{1.1}$$

The reorganization of free energy (λ) the driving force ($\triangle G^o$) and the electronic couplings between an initial and final state (H_{ab}). On their own, these parameters are computationally inexpensive to compute in contrast to computations using equation (1.1). Out of these three parameters, the electronic coupling is the only parameter directly proportional to the electron transfer rate; therefore, we can tune the electronic coupling to minimize or maximize the electron transfer. This has various applications, such as screening a database of dye-sensitized solar cells or optimizing an electron transfer between two covalent organic frameworks.

1.1.1 Dye Sensitized Solar Cells

A dye-sensitized solar cell (DSSC) is a solar energy conversion device where an organic dye covers the surface of Titanium dioxide (TiO_2) nanoparticles. The role of the dye in a solar cell is the absorption of sunlight to photoexcite an electron and transfer this excited electron to the TiO_2 nanoparticles. The dye taking this role reduces the necessary amount of semiconducting material and lowers the overall cost of the solar cell. After the photoexcitation

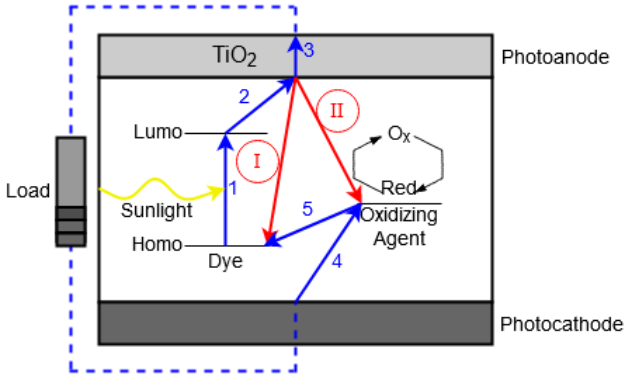

Figure 1.1 Diagram showing the pathway of an electron and the two recombination pathways within DSSCs. Adapted from Ref. 6

of the dye, we can see in Figure (1.1) that the electron follows the path of the blue arrow (1-5), transferring from the dye to the TiO_2 nanoparticles then flowing through an electric circuit and eventually back to the dye. After step 2, when the electron has transferred to the TiO_2 nanoparticles and before the electron transfers to the electric circuit, a process of recombination can occur down either two pathways: an inner pathway (I) or outer pathway (II). An electron on the inner pathway transfers straight back to the dye, while on the outer pathway, the electron transfers to the oxidized electrolyte.[6] Both of these recombination pathways represent losses in efficiency for DSSCs and are heavily dependent on the dye, especially the inner pathway. Therefore, an appropriate benchmark for the suitability of potential dyes would quantify this electron transfer between the TiO_2 nanoparticles and the organic dye. A method capable of finding the organic dye with the smallest electronic coupling for this inner pathway is of interest in designing DSSCs. A method such as this can

be extended to selecting chemical systems that seek to maximize an electron transfer rate by computation of electronic couplings.

1.1.2 Covalent Organic Frameworks

An example of a molecular system seeking an optimization process to find the maximum electron transfer within the system is covalent organic frameworks (COF). COFs are lightweight materials constructed by pre-selected organic subunits that dictate the chemical and physical properties of the COF.[7] In the case of two-dimensional COFs, by selecting subunits with certain specifications and reversible covalent bonds, the COF self-assembles into a columnar and symmetric COF with a unique pore size and shape, as seen in figure (1.2). The

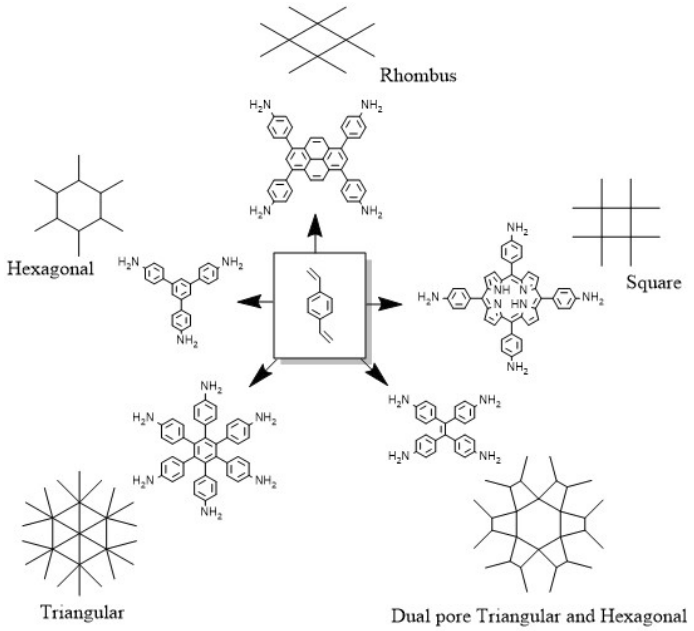

Figure 1.2 A selection of potential topologies accessible with a linear bifunctionalized linker and complementary linkers with other symmetries, resulting in COFs of different pore shape and symmetry.[8]

interactions between two COF layers heavily influence the physical properties of the COF, and this is of interest when seeking to develop a COF with semiconducting and photo-active properties.[8] Under these conditions, an important property is the electron transfer between two COF layers to determine its ability as a semiconductor. The orientation between the

COF layers is also a major contributing factor to consider when computing electronic couplings. Therefore, a method with the capabilities to compute the electronic couplings while taking into account the angle and distance between two COF layers should be selected. The method should also be computationally inexpensive when handling these complex materials at various orientations. The balancing of accuracy and computational viability is essential to any strategy, including the computation of electronic couplings.

1.2 Computational modeling of electronic couplings

Density Functional Theory (DFT) is one of the most common methods for computing energies from an electronic structure. While DFT is not the best option for all scenarios, DFT's balance between efficiency and accuracy contributes greatly to its popularity. This is largely due to the focus on the electron density of a system rather than the wave function compared to Schrodinger equation-based methods. The focus on electron density is based on the Hohenberg-Kohn theorem stating that there is a unique functional of the ground state electron density for every system.[9] Density-functional tight-binding (DFTB) is another quantum mechanical method that utilizes DFT to calculate electronic parameters and Hubbard parameters.[10] By approximating these parameters DFTB affords two key advantages over DFT. First, DFTB is more viable for large systems. As the systems get larger and more complex, the computational cost of DFT will scale faster than DFTB.[11] Second, because DFTB is a faster method, it is more suitable for projects with lengthy time scales such as screening through a large database of compounds.[11] However, these advantages come at the cost of accuracy due to DFTB's dependence on the quality of the electronic and Hubbard parameters. The accuracy of DFTB is also affected by any of the shortcomings that originate from the DFT method. Most notably, the self-interaction error stemming from the use of electron density to compute electron-electron interactions. Therefore, to compute electronic coupling using either DFT or DFTB, we must address this self-interaction error.

1.3 Constraint and Configuration Interaction

When computing the energy contribution from electron-electron interactions, $\hat{U}$, using a DFT method or a derivative of DFT, the key variable is electron density, $n_o(\vec{r})$.

$$\hat{H}\psi_o = \left[\hat{T} + \hat{V} + \hat{U}\right]\psi_o \tag{1.2}$$

$$\hat{U} = U[n_o\vec{r}] = \frac{1}{2}\iint \frac{n_o(r_1)n_o(r_2)}{r_{12}} dr_1 dr_2 \tag{1.3}$$

This can be seen in equation (1.3)[12] where the repulsive potential energy between two electrons, $n_o(r_1)$ and $n_o(r_2)$, is computed but the electron r_1 is present in electron density $n_o(r_2)$ and the same for r_2 in $n_o(r_1)$. This double-counting of electrons leads to an overestimation of the contribution coming from electron-electron interactions creating the self-interaction error. In DFT, a method has been developed to calculate the electronic couplings by implementing a constraint followed by a configuration interaction.[13] This constraint allocates charge to a pre-defined constrained region, and this process repeats, creating a multitude of states to represent "snapshots" of the electron transfer of interest. This process addresses the self-interaction error by implementing a formalism on the constrained region by setting the number of electrons on the region equal to a constant. In figure (1.3), a benzene dimer

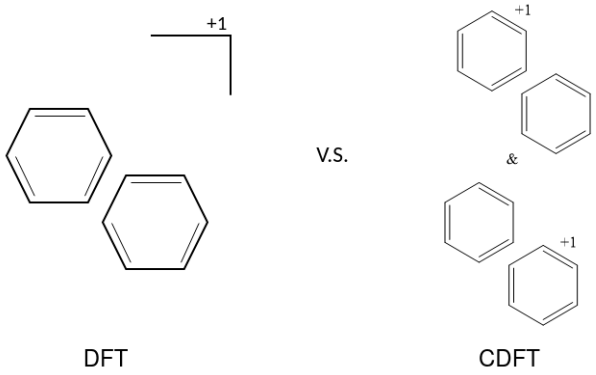

Figure 1.3 Benzene dimer example of charge allocation in DFT and CDFT

with a positive charge represented in both DFT and CDFT demonstrates that conventional DFT, and tangentially DFTB as well, can only distribute the charge over both benzenes.

This model is accurate when the two benzenes are close, but DFT will have this positive plus one charge over the entire system even when the benzenes are far apart. The issue has been account for by the formalism introduced by CDFT, which has forced the charge to the predefined constrained region. Then a small configuration interaction (see Chapter 2) is performed between these produced states to compute the electronic coupling. It is important to note that the formalism introduced by the constraint is incorrect when the benzenes are close; the configuration interaction computation corrects this. The following research is the implementation of this method that has been applied for DFT into DFTB, a concept suggested by Dr. Mathias Rapacioli[14] as another possible strategy to solve for electronic couplings more efficiently. The method development of this constrained density functional tight binding followed by a configuration interaction (CDFTB-CI) was in the quantum mechanical software package DFTB+.[12]

Chapter Two

Methods

2.1 Overview

Constrained density-functional tight-binding followed by a configuration interaction (CDFTB-CI) method begins with a conventional self-consistent charge density-functional tight-binding (SCC-DFTB) calculation solving for the energy for an approximation of the full Schrodinger equation 2.1.

$$\hat{H}\Psi = E\Psi \tag{2.1}$$

During this SCC-DFTB calculation, key variables and matrices are tracked, modified, and used to construct states representing snapshots of an electron pathway. Once the SCC-DFTB calculation has converged, we will have built the constrained states, and we can now perform the configuration interaction. To compute the electronic coupling (H_{AB}) of this electron transfer rate by a configuration interaction requires two constrained states to represent the beginning Ψ_A and an endpoint Ψ_B of an electron pathway.

$$H_{AB} = \left\langle \Psi_A \left| \hat{H} \right| \Psi_B \right\rangle \tag{2.2}$$

As an example, to find the electronic coupling for an electron transfer between two benzene's in a neutral benzene dimer as seen in Figure 2.1, a modified SCC-DFTB ground-state calculation for a benzene dimer is first performed. During this process, we will build two

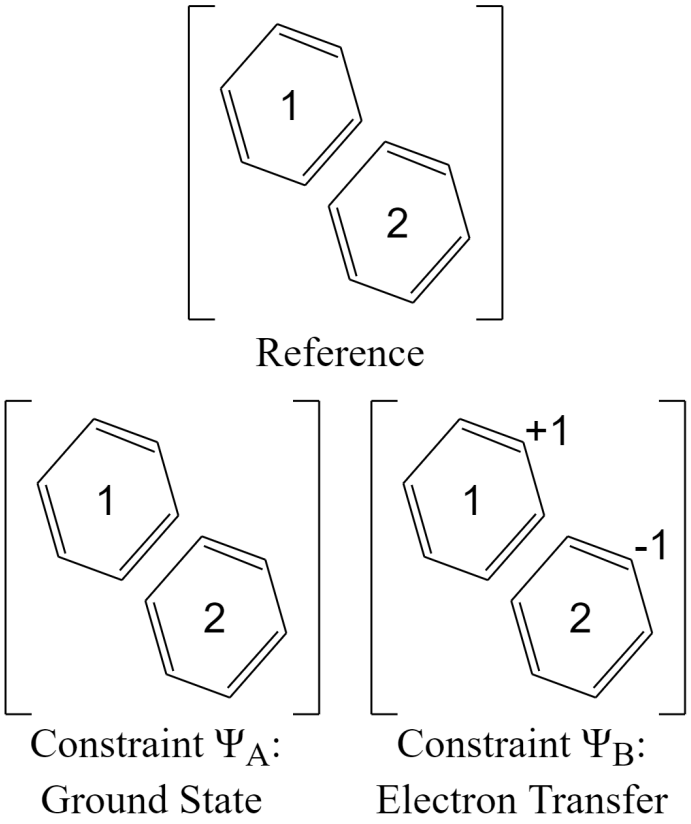

Figure 2.1 An example of constrained states using an electron transfer from benzene monomer 1 to benzene monomer 2 of a benzene dimer

constraints to represent the benzene dimer ground state and a state where the electron transfer has already occurred between benzene monomer one and benzene monomer two. With constraint states Ψ_A as the ground state and Ψ_B as the completed electron transfer built, we can perform a configuration interaction to compute the electronic coupling for this electron transfer. The following sections of chapter two will deconstruct this calculation by first giving a DFT background and its connections and differences to DFTB. There will also be a simple derivation of DFTB from DFT. Next is to undertake a step-by-step breakdown of the construction of the constraint and configuration interaction calculation that follows. Finally, we will briefly discuss the implementation of this CDFTB-CI method into DFTB+ from a coding perspective.

2.2 Density Functional Theory and Density Functional Tight Binding

2.2.1 Hohenberg and Kohn Theorems

Much of the framework of DFT was first established by Hohenberg and Kohn (HK) in 1964,[15] who considered an arbitrary number of electrons inside a box being subjected to an external potential $v(r)$ and sought the electronic energy for a non-degenerate ground state density. This derivation resulted in the following two theorems: Theorem 1 states that the external potential $v(r)$ and therefore the energy, is a unique function of the electron density $n(r)$, and Theorem 2 states that the density that minimizes the energy is the exact ground-state density. Even though the derivation assumed a non-degenerate ground state density, the theorems also work for a degenerate ground state density. The full derivation will not be shown here to avoid redundancy. Still, a simple derivation, with help from references,[16–19] is required in order to understand the theorems developed by HK.[15]

The HK Theorem 1's proof begins by considering an electron density of a non-degenerate ground state $n(r)$. Because of the significant mass difference between electrons and nuclei, the nuclei can be considered fixed by the Born-Oppenheimer approximation, which generates the static external potential $v(r)$. We then write the Hamiltonian from the Schrodinger equation [2.1] as

$$\hat{H}\Psi = \left[\hat{T} + \hat{U} + \hat{V}\right]\Psi \tag{2.3}$$

where $\hat{V}$ is the electron-electron interaction operator

$$\hat{V} = \int v(r)\psi^*(r)\psi(r)dr \tag{2.4}$$

while $\hat{T}$ and $\hat{U}$ are the kinetic energy operators. We will represent the ground state as Ψ and ψ as the wave function to denote the electronic density $n(r)$ as

$$n(r) = \langle \Psi, \psi^*(r)\psi\Psi \rangle \tag{2.5}$$

and the dependence of $n(r)$ on Ψ implies that $n(r)$ is functional of $v(r)$. Then to show that $v(r)$ is functional of $n(r)$, HK proceeded to use *reductio ad absurdum* based proof to demonstrate that the assumption that two external potential $v'(r)$ and $v(r)$ can have the same $n(r)$ leads to an inconsistency, establishing HK Theorem 1. Following the proof of HK theorem 1, HK continued by establishing that the kinetic and electron-electron interaction energies are also a function of $n(r)$, making $F[n(r)]$ the universal functional of the charge density, since Ψ is a functional of $n(r)$:

$$F\left[n(r)\right] = (\Psi, (\hat{T} + \hat{U})\Psi) \tag{2.6}$$

Hohenberg and Kohn then used the previous results, for a given $\nu(r)$, and created an energy functional.

$$E_\nu = \int v(r)n(r)dr + F[n] \tag{2.7}$$

To obtain the minimum in the above equation the number of particles must be kept constant and then let Ψ' be associated with a different external potential $v'(r)$ and therefore a different $n'(r)$.

$$\delta_v[\Psi'] = \int v(r)n'(r)dr + F[n'] > \delta_v[\Psi] = \int v(r)n(r)dr + F[n] \tag{2.8}$$

With $v(r)$ present on both sides of the inequality $delta_v[\Psi] \ > \ delta_v[\Psi']$ establishes that the ground state Ψ corresponds to the minimum E which is HK Theorem 2, also known as the DFT variational principle.

2.2.2 Kohn Sham method as a Basis for DFTB

The HK theorems prove that the electron density can completely determine the energy of a system; these theorems, however, do not provide a procedure to perform this calculation. A procedure known as local density approximation (LDA) was developed in the following year by Kohn and Sham (KS).[20] To understand how the KS method is used as a basis for DFTB, we have to derive the KS method in DFT.[21–24] The KS method starts by using a system

of non-interacting electrons subject to an external potential as a reference. Therefore, the following equations ignore electron-electron interaction terms, but the electron density we seek corresponds to a system of interacting electrons. With this taken into consideration, the HK universal functional can be rewritten in three key components.

$$F[n] = T_s[n] + J[n] + E_{xc}[n] \tag{2.9}$$

The first is T_s the kinetic energy of non-interacting electrons,

$$T_s[n] = \sum_{\imath}^{occ} \left\langle \Psi_\imath \left| \frac{1}{2}\nabla_\imath^2 \right| \Psi_\imath \right\rangle \tag{2.10}$$

then J is the coulomb interaction functional,

$$J[n] = \iint \frac{n(r)n(r')}{|r - r'|} dr dr' \tag{2.11}$$

and E_{xc} is the exchange-correlation energy functional; the later expression was obtained from considering a case of slowly varying densities. Here E_{xc} can be described in terms of exchange correlation energy per electron of a uniform electron gas (UEG).

$$E_{xc} = \int n(r)\varepsilon_{xc}^{UEG}[n(r)]dr \tag{2.12}$$

Then by utilizing equations 2.9, 2.10, and 2.11 within the DFT variational principle to develop an equation for the chemical potential (energy per unit of electron density),

$$\mu = \nu_{KS}(r) + \frac{\delta T_s[n]}{\delta n(r)} \tag{2.13}$$

with the KS effective potential.

$$v_{KS}(r) = v_{ext}(r) + \frac{\delta J[n]}{\delta n(r)} + \frac{\delta E_{ext}[n]}{\delta n(r)} = v_{ext}(r) + \frac{\delta J[n]}{\delta n(r)} + v_{xc} \tag{2.14}$$

The equation for the chemical potential 2.13 is proven by KS to be precisely the same as an equation produced from a system of non interacting electrons subject to an external potential, meaning $v = v_{KS}$. Therefore, for a known v_{KS} can be used to obtain $n(r)$ by solving the monoelectronic equation 2.16

$$\left[-\frac{1}{2}\nabla + \nu_{KS} \right] \Psi_\imath = \varepsilon_\imath \Psi_\imath \tag{2.15}$$

and setting

$$n(r) = \sum_{\imath=1}^{N_{\text{elec}}} |\Psi_\imath| \tag{2.16}$$

where N_{elec} is the fixed number of electrons. Equations 2.13-2.16 can be considered the KS equations, and by utilizing these equations, one can solve for the electron density that minimizes the energy. This process starts by first supplying an initial density $n_0(r)$ and using it to compute v_{KS} using the associated KS equation. With this computed v_{KS}, equations 2.15 and 2.16 can be used to compute a new $n(r)$ which will be used to compute a new v_{KS}. This cycle continues until a threshold condition is met, such as $(n_{\text{new}} - n_{\text{old}} \leq 10^{-8})$, determining convergence on an energy of the ground state density. Once this iterative process has concluded, the total energy can be computed using the following equation developed by KS.

$$E[n(r)] = \sum_{i}^{\text{occ}} \left\langle \Psi_\imath \left| -\frac{1}{2}\nabla^2 + \nu_{ext} + \frac{1}{2}\int \frac{n(r')}{|r-r'|}dr' \right| \Psi_\imath \right\rangle + E_{xc[n]} + \frac{1}{2}\sum_{\beta}^{N}\sum_{\alpha\neq\beta}^{N}] \frac{Z_\alpha Z_\beta}{|R_\alpha - R_\beta|} \tag{2.17}$$

It is important to note that the most challenging part of LDA-DFT is computing ν_{xc} because the exact form of the E_{xc} functional is not known. Therefore, what separates DFT methods is how the approximation of the E_{xc} is chosen and how the KS orbitals are represented.

2.2.3 DFTB

Now with LDA-DFT framework established, we can begin applying approximations to the KS scheme. The derivation of tight-binding parameters utilizing DFT was developed by Foulkes and Haydock[25] and has been reviewed by several articles.[10,11,22,26–30] To start, we rewrite the electronic structure to include a superposition of an reference density $n_0(r)$ with a small fluctuation $\delta n(r)$,

$$n(r) = n_0(r) + \delta n(r) \tag{2.18}$$

this can then be inserted into equation 2.17 to develop the following energy equation of DFTB.

$$E^{\mathrm{DFTB}}[n_0(r)+\delta n(r)] = \sum_{\imath}^{occ}\left\langle \Psi_i \left| -\frac{1}{2}\nabla + \nu_{ext} + \frac{1}{2}\int \frac{n_0'}{|r-r|} + \nu_{xc}[n_0] \right| \Psi_\imath \right\rangle - \frac{1}{2}\iint \frac{n_0' n_0}{|r-r'|} dr dr' + E_{xc}[n_0] - \int \nu_{xc}[n_0] n_0 dr + E_{nn} + \frac{1}{2}\iint \left(\frac{n_0' n_0}{|r-r'|} + \frac{\delta^2 E_{xc}}{\delta n \delta n'}\bigg|_{n_0} \right) dr dr' \tag{2.19}$$

The energy equation of DFTB can be simplified further into equation 2.20

$$E^{\mathrm{DFTB}}[n_0(r)+\delta n(r)] = \sum_{\imath}^{occ}\left\langle \Psi_\imath \left| \hat{H}^0 \right| \Psi_\imath \right\rangle + E_{rep}[n_0] + E_{2nd}[n_0(r), \delta n(r)] \tag{2.20}$$

where the reference Hamiltonian, $\hat{H}^0$, is written as,

$$\hat{H}^0 = -\frac{1}{2}\nabla + \nu_{ext} + \frac{1}{2}\int \frac{n_0'}{|r-r|} + \nu_{xc}[n_0] \tag{2.21}$$

and this summation of $\hat{H}^0$ in equation 2.20 is analogous to the sum over the energies of all occupied orbitals. The second term in equation 2.20 is the repulsive contribution E_{rep} term, which is represented by the following equation 2.22.

$$E_{\mathrm{rep}}[n_0] = -\frac{1}{2}\iint \frac{n_0' n_0}{|r-r'|} dr dr' + E_{xc}[n_0] - \int \nu_{xc}[n_0] n_0 dr + E_{nn} \tag{2.22}$$

The third term of equation 2.20, E_{2nd}, represents the corrections to the fluctuations in the electronic density.

$$E_{2nd}[n_0(r), \delta n(r)] = \frac{1}{2}\iint \left(\frac{n_0' n_0}{|r-r'|} + \frac{\delta^2 E_{xc}}{\delta n \delta n'}\bigg|_{n_0} \right) dr dr' \tag{2.23}$$

With the DFTB energy functional established, it is important to note that the KS orbitals in DFTB are represented by the linear combination of atomic orbitals (LCAO) centered on the nuclei. With basis functions denoted by ϕ_ν and expansion coefficients $C_{i\nu}$ the KS orbitals can be written in the form.[14]

$$\psi_\imath(r) = \sum_{\nu}^{N} C_{\imath\nu}\phi_\nu\left(r - R_\alpha\right) \tag{2.24}$$

Then from this LCAO model one can obtain the secular problem

$$\sum_{\nu}^{N_{\text{occ}}} C_{\nu\nu}(H_{\mu\nu} + S_{\mu\nu}) = 0 \tag{2.25}$$

where $S_{\mu\nu}$ is the atomic overlap matrix, and $H_{\mu\nu}$ is the Hamiltonian matrix with $\mu \, \epsilon \, \alpha$ and $\nu \, \epsilon \, \beta$ meaning atomic orbital μ belongs to atom α, and atomic orbital ν belonging to β. The Hamiltonian matrix is read as

$$H_{\mu\nu} = H^0_{\mu\nu} + H^1_{\mu\nu} \tag{2.26}$$

where the reference Hamiltonian, $H^0_{\mu\nu}$, is built using equation 2.21 and the Hamiltonian elements that depends on the Mulliken charges, $H^1_{\mu\nu}$, is built using equation [2.27].

$$H^1_{\mu\nu} = \frac{1}{2} S_{\mu\nu} \sum_{\xi}^{\text{atoms}} (\Gamma_{\alpha\xi} + \Gamma_{\xi\beta}) \tag{2.27}$$

This dependence on the Muliken charges means there is also a dependence on the molecular orbital coefficients and thus requires this computation to be solved self consistently, hence self consistent charge (SCC). With an established energy functional and representation of the KS orbitals, the CDFTBCI method can be properly discussed.

2.2.4 Introducing Constraints and Configuration interaction into DFTB framework

Construction of the Constraint

This implemented constraint model aims to create constrained states built from a reference to replicate snapshots of a beginning and endpoint of an electron pathway to simulate an electron transfer. The application of this model redefines the wave function ψ of an electron transfer to be expressed by a basis, Φ^I, constrained states.

$$\Psi = \sum_{I}^{N_{\text{frag}}} b_I \Phi^I \tag{2.28}$$

The decomposition of a molecular system is now represented by a number of constrained states, N_{frag}, which each have localized charge only a fragment of the system. Therefore,

each charge localized configuration Φ^I is a single Slater determinant built from a constrained SCC-DFTB calculation. The basis set in which this constraint state is made from is based upon what basis set the Hamiltonian is built from, and in the case of DFTB, it is a basis set, ϕ_i^I, of atomic orbitals. A corresponding Lagrangian represents this constraint calculation in equation 2.29.

$$\mathcal{L} = E^{\mathrm{DFTB}}(\phi_i^I) + \sum_{ij} \Lambda_{ij}^I \left(\langle \phi_i^I | \phi_j^I \rangle - \delta_{ij} \right) + V^I \left(N_D - N_C \right) \tag{2.29}$$

Where N_D is the desired number of valence electrons on a given fragment and N_C is the number of computed valence electrons on the same fragment from the constrained calculation. The first term of the equation 2.29 is the ground state energy of the system supplied by DFTB, the third term is the constraint with the Lagrange multiplier, V^I, ensuring charge localization on fragment I. The second term provides the orthonormality of the constraint. Since SCC-DFTB supplies the first term, and N_D is established beforehand for a given constrained state, the only variables that the CDFTB-CI method needs to compute are N_C and V^I. A localization scheme[14] based upon the Mulliken charge definition will be used to calculate N_C, as the Mulliken charge definition is utilized in the partial charge of SCC-DFTB. This choice leads to the following expression for N_C

$$\sum_{i\mu\nu} n_i C_{i\mu}^I C_{i\nu}^I P_{\mu\nu}^I = N_C \tag{2.30}$$

where P is a projection matrix representing the density on fragment I

$$P_{\mu\nu}^I = \begin{cases} 0 \text{ if } \mu \notin \mathrm{I} \text{ and } \nu \notin \mathrm{I} \\ S_{\mu\nu} \text{ if both } \mu \in \mathrm{I} \text{ and } \nu \in \mathrm{I} \\ \frac{1}{2} S_{\mu\nu} \text{ for other case } (\mu \in \mathrm{I} \text{ or } \nu \in \mathrm{I}) \end{cases} \tag{2.31}$$

The $H_{\mu\nu}$ matrix from the secular equation, when the constraint is applied, becomes

$$H_{\mu\nu} = H_{\mu\nu}^0 + H_{\mu\nu}^1 + V^I P_{\mu\nu} \tag{2.32}$$

This secular equation must now be solved self-consistently over the atomic charges with $H_{\mu\nu}$ containing an unknown V^I.

Three methods are presented by Rapcioli that can overcome convergence issues. First is a method utilized by Van Voorhis and Wu[13] for constrained DFT based around an inner loop and outer loop. The inner loop has the Hamiltonian computed with fixed atomic charges, and the Lagrange multiplier is modified so that the AOs diagonalizing the Hamiltonian satisfy the charge localization constraint. The outer loop is the self-consistent loop over the atomic charges. The second method is the inverse of the first method. The inner loop ensures self-consistency over the Mulliken charges, and the outer loop allows for a determination of the Lagrange multiplier. The third method, which is utilized by Rapcioli,[14] involves an iterative procedure that evolves the MOs to change the charge on fragment I and solves for the Lagrange multiplier using a second-order equation equivalent to the Rickert algorithm. We chose the first method since the Van Voorhis and Qin Wu takes on the inner and outer loop fit the structure of DFTB+ without sacrificing convergence efficiency

Application of the Constraint in DFTB+

The inner loop and outer loop strategy chosen means that the constraint loop is implemented directly inside the SCC loop. A loop is referring to the iterative processes of either the SCC-DFTB computation or the construction of constraint. This means that an SCC loop will have multiple SCC iterations performed before convergence. Contained in all the SCC iterations is an entire constraint loop with multiple constraint iterations performed before reaching convergence itself.

The specific location of the constraint loop within an SCC iteration is between the Hamiltonian computation and the Hamiltonian's diagonalization. We chose this location because we received the necessary variables at their correct stage, but they have not yet been utilized within the SCC iteration. This placement is important because we want the SCC loop to be using the Hamiltonian modified by equation 2.32 for the SCC-DFTB computation to

produce an energy representative of the constraint. The information supplied by each SCC iteration are parameters of the constraint defined in the input file, the Hamiltonian, the overlap matrix, and the occupation number. The parameters specified in the input file are the region of the constraint and the constraint value representing the number of electrons applied to the constrained region. A preliminary step specific to the stage of the calculation preps this information. What initial steps are performed is determined by checkpoint system tracking events that occur during the calculation. Examples of checkpoints would be the first SCC iteration, the first constraint iteration, or the transition from an SCC iteration to the next SCC iteration. These steps are only performed from a coding perspective to avoid double counting, skipping key events, or removing necessary variables. A majority of these steps will not be discussed here except for a few but critical preparatory steps.

The first constraint iteration of the first SCC iteration has the Lagrange multiplier (V^I) set equal to 0.1. Setting it equivalent to a number greater than zero perturbs the Hamiltonian to initiate the constraint construction. Then each sequential constraint iteration and SCC iteration will be using a progressively better V^I. The second is that the Hamiltonian is reset to an initial Hamiltonian supplied at the beginning of every SCC iteration for every constraint loop. This step here is the source of the feedback loop between the SCC loop and the constraint loop. A case in point, the first SCC iteration supplies a Hamiltonian, and that Hamiltonian is saved as H_{base}. All modifications done by the V^I and the projection matrix in equation 2.32 are done on this H_{base}. Then, when convergence occurs for a constraint loop, that final modified Hamiltonian is not reset and return to the SCC iteration. This modified Hamiltonian with a localized charge on a fragment requires readjustments to $H^1_{\mu\nu}$ by the SCC loop due to $H^1_{\mu\nu}$ dependence on the Mulliken charges. Therefore, the next SCC iteration supplies a new H_{base} to the constraint loop. This process continues until convergence.

A single iteration of the constraint loop begins by building the projection matrix from the overlap matrix based on equation 2.31. It's important to note that this needs to be

done only once per constraint loop since the overlap matrix will remain unchanged during this loop. With the projection matrix built, the variables $H^0_{\mu\nu}$ plus $H^1_{\mu\nu}$ is represented by the previously mentioned H_{base} therefore, the last variable inputted into equation 2.32 is the Lagrange multiplier V^I. The V^I within code version of equation 2.32 is representative $(\lambda + d\lambda)$ where λ is the V^I, and $d\lambda$ is the change that will be eventually applied entirely to the λ when the constraint loop converges. With the modified Hamiltonian built, we diagonalize the Hamiltonian to produce its eigenvectors. The eigenvectors are then inputted into equation 2.30 to compute N_C. A subroutine is enacted at this step, which is broken down further by the "Find the LaGrange Multiplier" section to compute the $d\lambda$. This process is repeated until the difference between $d\lambda$ and the $d\lambda$ from the previous iteration is smaller than a pre-defined threshold indicating convergence of the constraint loop within an SCC iteration. Then $d\lambda$ is applied to λ, and $d\lambda$ is reset for the constraint loop in the following SCC iteration. Finally, after the repetition of this process from SCC iteration to SCC iteration, the constraint is constructed when the SCC loop converges.

Finding the Lagrange Multiplier

The Lagrange multiplier V^I or $(\lambda+d\lambda)$ we are looking for is the one that minimizes the energy of the constraint $\mathcal{L}$. Fortunately, the work from Wu and Yang[24] demonstrates that the function $\mathcal{L}[(\lambda + d\lambda)]$ is concave; therefore, it has only one minimum. The strategy employed to find this single minimum is adapted from a process from the quantum mechanical computing software NWCHEM.[31] This process can be broken into two modules, a construction module establishing the bounds that contain the minimum and the convergence module that constricts those bounds until converging on the minimum. Before going further, there are key variables that need to be established. First, x_1 and x_2 are the lower and upper bounds of the bracket that will contain the minimum, and the minimum is a $(\lambda + d\lambda)$ that produces

an N_C that approaches N_D. Second are the derivatives, dl for the first derivative

$$dl = N_D - N_C \tag{2.33}$$

and d^2l for the second derivative, which at the moment is set equal to 1. There is also dl_{old} to represent the previous best first derivative. Typically dl_{old} is the previous iteration's dl, but dl won't be saved in dl_{old} when there was a poor adjustment made when seeking the minimum. The third is the $d\lambda$ variable representative of the change applied to the Lagrange multiplier λ upon convergence. It is also important to note that this technique solves for the $d\lambda$ that when applied to λ is the minimum.

The construction module's goal is to have x_1 represent unique $d\lambda$ that produces an N_C that is less than N_D and x_2 representative of a unique $d\lambda$ that produces an N_C that is greater than N_D, indicating containment of the minimum. The beginning of the construction module starts by setting $x1$ equal to 0, x_2 equal to -dl/d^2l, and the $d\lambda$ set equal to x_2. The adjustments from this point forward are to maintain the state where x_2 is between the minimum and x_1. This establishes a directionality base upon x_2, dl, and dl_{old} utilizing two critical pieces of logic. The first reason is that as you approach the minimum of a concave function, the first derivative approaches zero. Therefore, when the absolute of dl is less than the absolute of dl_{old} indicates that x_2 is approaching the minimum. Within this case, x_2 will be adjusted in that direction. Then in the opposite case where it indicates that x_2 is moving away from the minimum. This case requires x_1 and x_2 to be flipped to reestablish the directionality of x_2 heading towards the minimum. This process continues until the criteria based upon the second piece of logic are met. This criterion uses the sign of the gradient to indicate when x_2 has passed the minimum. When x_2 is still approaching, the minimum dl and dl_{old} will have the same sign, but when x_2 passes, the minimum dl will change sign and be opposite in sign to dl_{old}.

The convergence module's goal is to squeeze the bracket onto the minimum. This squeezing process is done by computing a $d\lambda$ that is contained within the bracket. Then determining

where the $d\lambda$ is in the bracket regarding x_1, x_2, and the minimum. If it is determined that $d\lambda$ is between x_1 and minimum, then x_1 is shifted to this new $d\lambda$ position, and the same goes for x_2 if $d\lambda$ is between x_2 and the minimum. This decision process is only possible by setting dl_{old} equal to dl when the computed $d\lambda$ is between x_1 and the minimum. Therefore we can use the sign of dl_{old} to determine whether it's between x_1 and the minimum or x_2 and the minimum. This process continues until x_1 and x_2 converge on the minimum and $d\lambda$ is added to λ.

Configuration Interaction of the Constrained states

Completing the self-consistent charge constrained density-functional tight-binding (SCC-CDFTB) computations, a set of MO's ϕ_i^I have been obtained. These MO's are used to build the charge-localized configurations of each constraint Φ^I from equation 2.28, where the coefficient b_I of Φ^I are obtained by solving the CI-like scheme.[14]

$$\begin{bmatrix} H_{11} & H_{12} \\ H_{21} & H_{22} \end{bmatrix} \begin{pmatrix} b_1 \\ b_2 \end{pmatrix} = E \begin{bmatrix} S_{11} & S_{12} \\ S_{21} & S_{22} \end{bmatrix} \begin{pmatrix} b_1 \\ b_2 \end{pmatrix} \tag{2.34}$$

The S_{IJ} is the two-configuration overlap $\langle \Phi^I | \Phi^J \rangle$ and H_{II} is the energy of the configuration Φ^I which SCC-CDFTB has already calculated. The electronic coupling is the off-diagonal elements H_{IJ} which is calculated by

$$H_{IJ} = \frac{1}{2}\left(H_{II} + H_{JJ} + N_C^I V^I + N_C^J V^J\right) S_{IJ} - \frac{1}{2}\left(V^I \langle \Phi^I | \hat{P}^I | \Phi^J \rangle + V^I \langle \Phi^I | \hat{P}^J | \Phi^J \rangle\right) \tag{2.35}$$

From a coding, perspective this is relatively simple to implement since SCC-CDFTB has computed all the elements; hence, to obtain the electronic coupling, only equation 2.35 needs to be implemented. However, the difficulty to have this work is it this requires two SCC-CDFTB computations to run back to back to compute two constrained configurations Φ^I and Φ^J. The sequential evaluation and storage of multiple constrained states for the construction and solution of the CI equations remain a work in progress.

Chapter Three

Results

This evaluation aims to check the SCC-CDFTB method's proficiency in constructing constrained configurations. We measure this proficiency in terms of whether the technique can distinguish each constrained state from the reference ground state, from the other constrained configurations, and whether these constrained states are reasonable representations of their associated charge localized configuration. The guidelines for this measurement will be the energy difference between a configuration's energy and reference ground state energy, charge difference between the constraint region (C) and for the unconstrained region (U), the number of calculated electrons (N_C) on C, and the Lagrange Multiplier $\left(V^I\right)$.

Two sets of molecular systems are utilized in this evaluation, a homogeneous set and a heterogeneous set. The homogeneous set is a water dimer $(H_2O)_2$ and a hydrogen sulfide dimer $(H_2S)_2$. The heterogeneous set is a tetrafluoroethylene-ethylene dimer $(C_2F_4 \cdots C_2H_4)$ and water-hydrogen sulfide dimer $(H_20 \cdots H_2S)$

We will construct three constrained configurations for both the homogeneous dimer set and the heterogeneous dimer set. The constraint will be applied to one of the molecules of the dimer, placing that molecule in region C and the other molecule of the dimer in region U. A constraint value of 1, 0, or -1 will be applied to C, where the constraint value equals the number of electrons being transferred to C from U. This means for a constraint value 1 an electron is transferred from U to C (C^-U^+), for 0 no electrons are transferred between C

and U (CU), and for -1 an electron is transferred from C to U (C^+U^-).

Each SCC-CDFTB computation was performed with a DIIS mixer with the DFTB+ default initial mixing parameter of 0.2, three generations considered for mixing, and is used at the start of the computation (see Discussion in chapter 4). We also set the electronic temperature of the molecular system equal to 300K which will distribute single-particle levels according to a Fermi distribution. Also, we increased the maximum number of SCC iterations to 1000 due to the constraint complicating convergence. We performed these SCC-CDFTB computations at different separations between the dimers in increments of 0.1 Å from 0.0 Å to 10.0 Å.

3.1 Homogeneous Dimer Cases

The homogeneous dimers are important in evaluating SCC-CDFTB due to the relation of (C^- U^+), (C^+ U^-), and the symmetry of a homogeneous molecular system. From this symmetry, we expect constrained configurations with a constraint value of 1 and -1 to have the same energy; their Lagrange multipliers are predicted to be similar in value. The same is expected to be true for the charge difference between C and U. For a configuration with a constraint value of 0; the density should be similar to the reference ground state density. The images in Figure 3.1 were built using the molecular modeler Avogadro[32] and with their geometry optimized by Q-chem.[33] The Q-chem geometry optimizations used an exchange functional omegab97x-d and a basis set 6-31+G*. Also, the geometries highlighted in Figure 3.1 are examples of geometries utilized in the homogeneous computations. This geometry is also used as an initial reference geometry to produce all separations between the monomers from 0.0 Å to 10.0 Å.

The energy difference referred to in Figures 3.2 and later in the heterogeneous Figure 3.5 is the energy of the constrained configuration (H_{II}) subtracting the reference ground state energy ($E^{SCC-DFTB}$). For the water dimer in Figure 3.2a only at low separations between

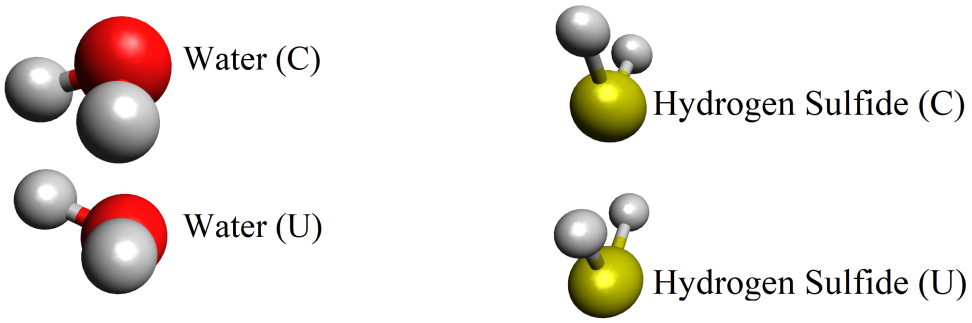

(a) Water Dimer **(b)** Hydrogen Sulfide Dimer

Figure 3.1 Molecular models of a water dimer and a hydrogen sulfide dimer

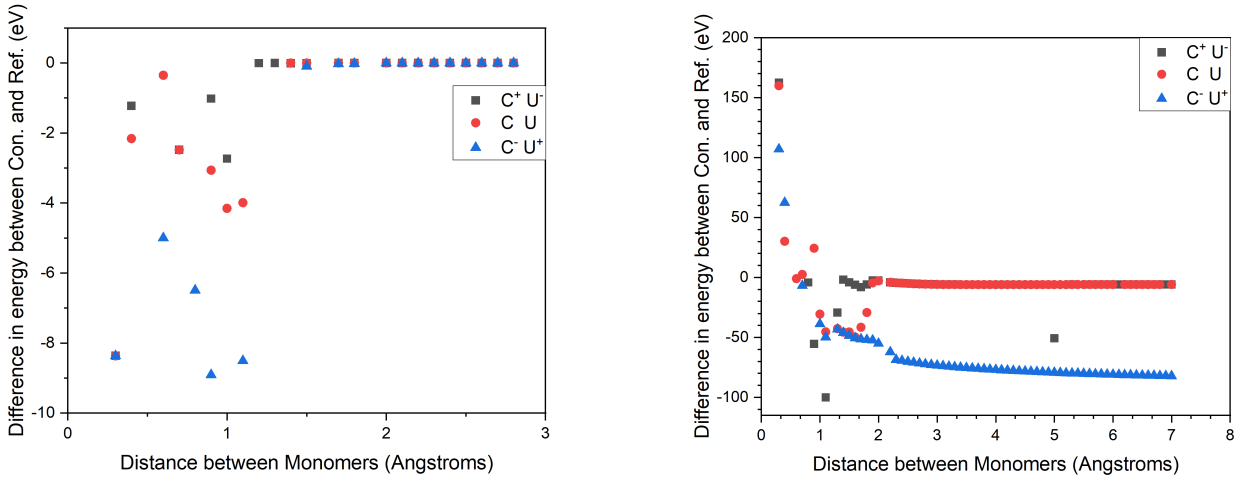

(a) Water Dimer **(b)** Hydrogen Sulfide Dimer

Figure 3.2 Energy difference of multiple constrained states to the reference ground state energy across different separations between each monomer for a water dimer and hydrogen sulfide dimer

0.3 Å and 1.2 Å, are the only separations where the constraint values 1 (C^- U^+), 0 (C U), or -1 (C^+ U^-) have distinguishable energy values from the reference ground state energy of water. Beyond separations of 1.2 Å all constrained configurations had energies equal to ($E^{SCC-DFTB}$), and therefore appear as 0.0 eV on Figure 3.2a. For the hydrogen sulfide dimer in Figure 3.2b all constraint configurations have a meaningful difference in energy from reference ground state energy. However, beyond separations of 2.2 Å, constrained configurations with a constraint value of -1 and 0 are both equal to each other with an average energy of -5.7 eV difference to reference. This differs significantly from the average energy differ-

ence to reference of −77.7 eV at the same separations for a constrained configuration with a constraint value of 1.

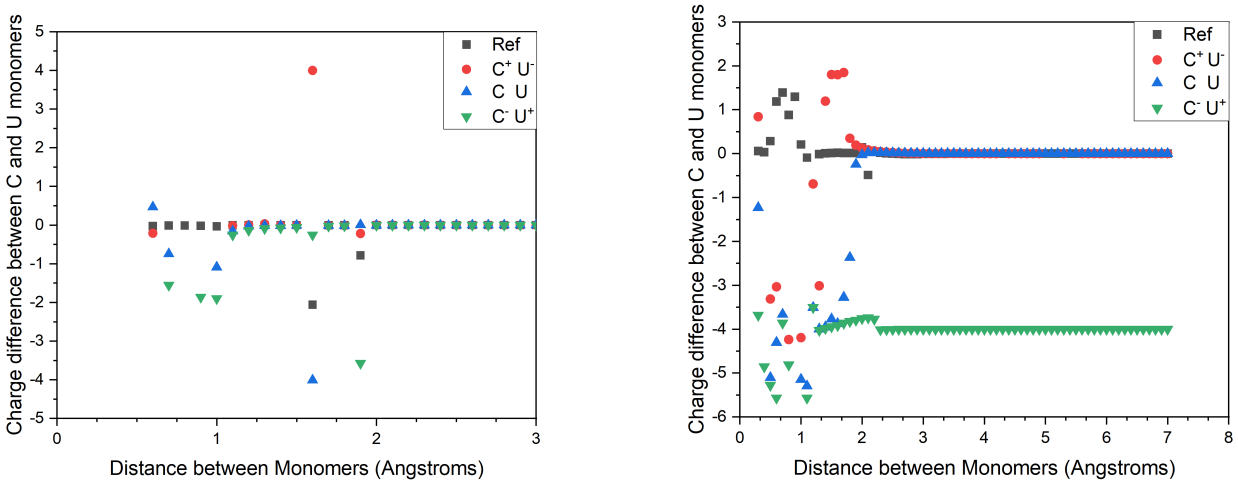

(a) Water Dimer **(b)** Hydrogen Sulfide Dimer

Figure 3.3 Charge difference between a monomer in region C and a monomer in region U for all constrained states and reference across different separations between monomers for a water dimer and hydrogen sulfide dimer

This trend is repeated similarly in Figure 3.3a and in Figure 3.3b when looking at the charge difference between monomers in region C and monomers in region U. In the case for the water dimer in figure 3.3a for a constrained configuration with constraint values 1, 0, or −1, the charge goes to 0.0 when at a separation more than 1.1 Å. For the hydrogen sulfide dimer in figure 3.3b when looking at separations above 2.2 Å, the average charge on constraint region C for constraint values 1, 0, and −1 constrained configuration was 4.000, 0.002, and 0.10 respectively. The reference ground state of the hydrogen sulfide dimer had a charge difference of −0.001 at these corresponding separations.

By taking note of the target number of electrons on the constrained region (C) on both a water dimer and hydrogen sulfide dimer, a configuration with a constraint value of 1 targets 9 electrons, a constraint value of 0 targets 8 electrons, and a constraint value of −1 targets 7 electrons. Then the number of calculated electrons N_C from Table 3.1 for each constrained configuration for both a water dimer and a hydrogen sulfide dimer have close to the correct

Property	CV−1	CV0	CV1
$(H_2O)_2$ $\langle N_C \rangle$	7.154985012	7.912562251	9.042605146
$(H_2O)_2$ σ_{N_C}	0.751048163	0.74064949	0.436414702
$(H_2O)_2$ $\langle V^I \rangle$	0.130384901	0.067945854	−0.086283247
$(H_2O)_2$ σ_{V^I}	0.616738151	1.178369086	0.235560575
$(H_2S)_2$ $\langle N_C \rangle$	6.913289152	7.883702262	9.844367184
$(H_2S)_2$ σ_{N_C}	1.015974751	0.90288892	1.812387777
$(H_2S)_2$ $\langle V^I \rangle$	0.228190564	0.058426814	−1.692722067
$(H_2S)_2$ σ_{V^I}	0.873015027	2.419750546	0.502114901

Table 3.1 Statistical analysis of the number of calculated electrons (N_C) and Lagrange Multiplier (V^I) for each constraint calculation across different separations between monomers for a water dimer and hydrogen sulfide dimer

number of electrons with one exception. The constraint configuration with a constraint value of 1 for hydrogen sulfide dimer, approaches 10 electrons instead of 9. For the Lagrange multiplier, a configuration with a constraint value −1 and 1 are opposite in sign but only moderately overlap in magnitude. A constraint value of 0 constrained configuration for both a water dimer and hydrogen sulfide dimer on average is closer to 0.

3.1.1 Heterogeneous Dimer Cases

The purpose of the heterogeneous dimers in evaluating SCC-CDFTB is again focused squarely around constrained configurations with a constraint value of 1 and −1. Compared to the homogeneous case, the asymmetry of a heterogeneous dimer emphasizes that a constrained configuration with a constraint value 1 is predicted to differ significantly from one with a constraint value of −1. Specifically, the constraint value that transfers an electron to the electron acceptor monomer from the electron donor monomer will be the lowest energy-constrained configuration. The Lagrange multiplier of constraint value 1 and −1 configura-

tions in the heterogeneous case is expected to vary significantly in magnitude. Similarly, in the homogeneous case, the heterogeneous constraint value of 0 constrained configuration is expected to be similar to the reference ground state density. These images in Figure 3.4 of tetrafluoroethylene-ethylene dimer and water-hydrogen sulfide dimer were built using Avogadro, geometry optimized through Q-chem, and are also examples of geometries utilized in the heterogeneous computations.

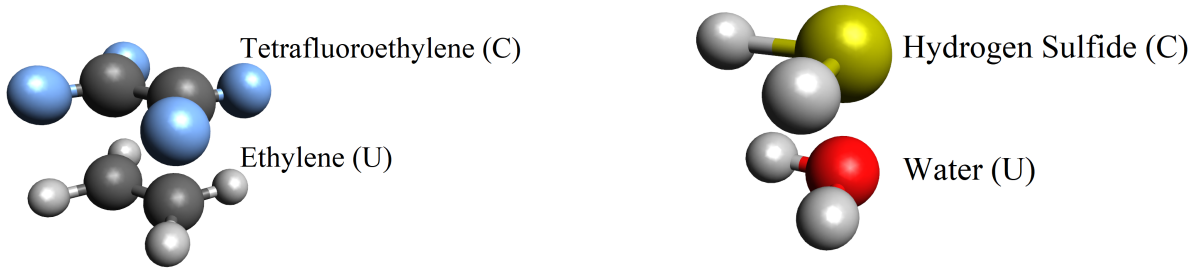

(a) Tetrafluoroethylene-Ethylene Dimer **(b)** Water-Hydrogen Sulfide Dimer

Figure 3.4 Molecular models of a tetrafluoroethylene-ethylene dimer and water-hydrogen sulfide dimer.

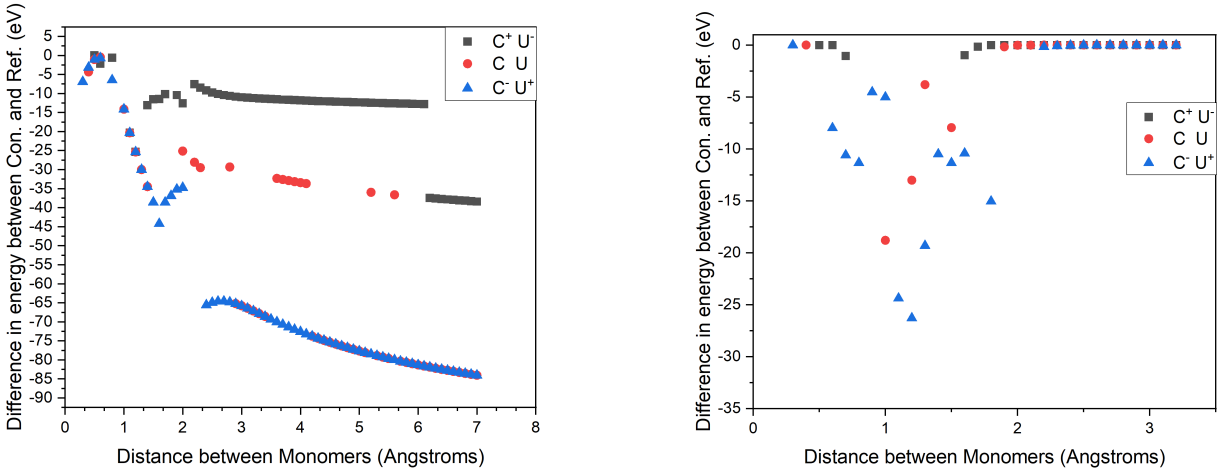

(a) Tetrafluoroethylene-Ethylene Dimer **(b)** Water-Hydrogen Sulfide Dimer

Figure 3.5 Energy difference of multiple constrained states to the reference ground state energy across different separations between each monomer for a tetrafluoroethylene-ethylene dimer and water-hydrogen sulfide dimer

The tetrafluoroethylene-ethylene dimer in Figure 3.5a beyond a separation of 2.4 Å has

distinct constrained configurations for constraint values 1 and −1 at around −70 eV and −10 eV. The constraint value of 0 case jumps between −33 eV and the constraint value of 1 region at −70 eV at these same separations. In Figure 3.5b, the only separation distances where the constrained configurations have different energies from reference is between 0.5 Å and 1.8 Å. Otherwise, the energies of the constrained configurations are equal to the reference ground state energy.

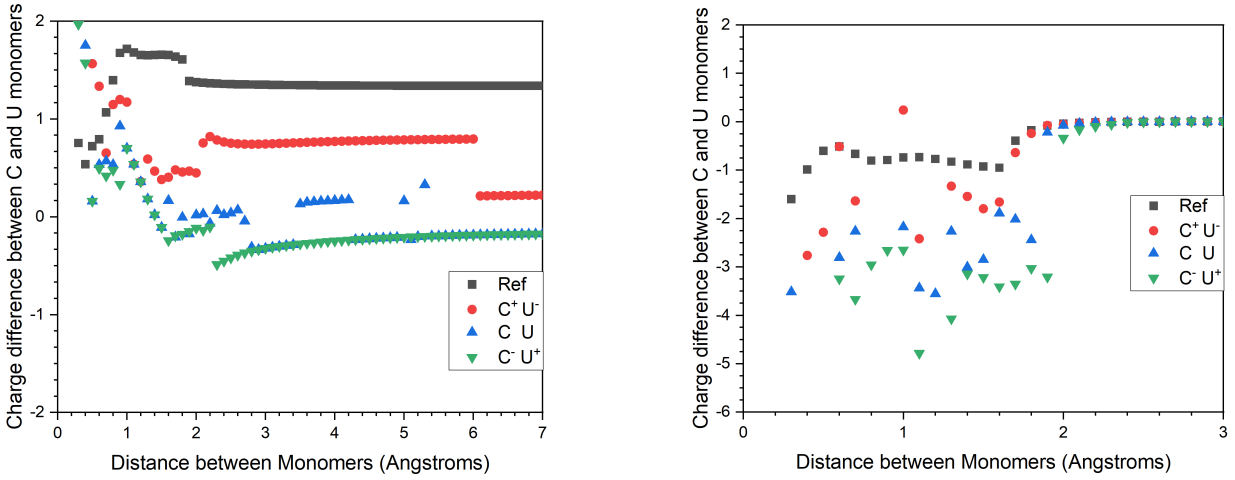

(a) Tetrafluoroethylene-Ethylene Dimer **(b)** Water-Hydrogen Sulfide Dimer

Figure 3.6 Charge difference between a monomer in region C and a monomer in region U for all constrained states and reference across different distances between monomers for a tetrafluoroethylene-ethylene dimer and water-hydrogen sulfide dimer

The pattern from Figure 3.5a is replicated in Figure 3.6a reinforcing the distinction between constrained configurations with constraint values −1 and 1 for the tetrafluoroethylene-ethylene dimer. For the separations above 2.4 Å, the constraint value 1 case has a charge difference of about −0.24. For constraint value −1, a charge difference of 0.7 dropping down to 0.21 when above separation of 6.1 Å. Additionally, the charge difference of constraint value 0 constrained configuration bounces between 0.15 and −0.24. The water-hydrogen sulfide dimer in figure 3.6b we can slightly differentiate the charge difference of each constrained configuration from each other between separations of 0.3 Å and 2.3 Å. This differentiation of constrained configuration loosely follows the order in figure 3.6a where constraint value

-1 charge difference is less than the charge difference of constraint value 0 which is less then constraint value of -1 charge difference.

Property	CV-1	CV0	CV1
$C_2F_4 \cdots C_2H_4$ $\langle N_C \rangle$	34.93875326	36.46179505	37.10166783
$C_2F_4 \cdots C_2H_4$ σ_{N_C}	0.806402582	1.418572387	1.364656523
$C_2F_4 \cdots C_2H_4$ $\langle V^I \rangle$	-0.824215433	-1.512764958	-1.579466836
$C_2F_4 \cdots C_2H_4$ σ_{V^I}	0.744380989	1.103607558	0.523220773
$H_20 \cdots H_2S$ $\langle N_C \rangle$	6.934996012	7.95428062	9.226984724
$H_20 \cdots H_2S$ σ_{N_C}	0.416938689	0.420699705	0.914575243
$H_20 \cdots H_2S$ $\langle V^I \rangle$	-0.094458137	2.019327236	-0.335932155
$H_20 \cdots H_2S$ σ_{V^I}	0.990191558	2.551945335	0.511426362

Table 3.2 Statistical analysis of the number of calculated electrons (N_C) and Lagrange Multiplier (V^I) for each constraint calculation across different separations between monomers for a tetrafluoroethylene-ethylene dimer and a water-hydrogen sulfide dimer

To discuss N_C of Table 3.2 first, we need to establish the target number of electrons N_D of tetrafluoroethylene-ethylene dimer and water-hydrogen sulfide dimer. For tetrafluoroethylene-ethylene dimer a constraint value -1 target is 35 electrons, a constraint value 0 target is 36 electrons, and a constraint value 1 target is 37 electrons. For water-hydrogen sulfide dimer a constraint value -1 target is 7 electrons, a constraint value 0 target is 8 electrons, and a constraint value 1 target is 9 electrons. Based on the average N_C and the standard deviation, each constraint configuration is approaching its target. The Lagrange multiplier for constraint values -1 and 1 of both heterogeneous dimers the averages differ as expected of a heterogeneous molecular system.

Chapter Four

Discussion

The metric used in evaluating the self-consistent charge constrained density functional tight bind (SCC-CDFTB) method was its capabilities to distinguish each constrained configuration from the reference ground state, from the other constrained configurations, and for them to be reasonable representations of charge localized configurations. This is because the SCC-CDFTB method aims to construct snapshots of a beginning and endpoint of an electron transfer. The formalism added by the constraint will skew the accuracy of the representation of the charge localized configuration. Therefore, the question is how reasonable the SCC-CDFTB method represents constrained configurations of the homogeneous dimers and heterogeneous dimers.

First are the homogeneous cases, a water dimer and a hydrogen sulfide dimer. The symmetry of a homogeneous dimer has a predictable impact on the constrained configuration. When the constrained region C is symmetric to the unconstrained region U, meaning E(C) = E(U) therefore $E(C^{-}U^{+}) = E(C^{+}U^{-})$. When comparing the energy of the constrained configurations energies to the reference in Figures 3.2, all water constrained configurations converged to the reference ground state energy, and for the hydrogen sulfide dimer all constrained configurations were distinctive from the reference ground state for constraint values of 1, 0, and -1. For a constrained configuration with constraint value 0 and -1 for the hydrogen sulfide dimer, the constraint value -1 seems to be collapsing into the configuration

of a constraint value 0 while constraint value of 1 was truly distinct. In Figure 3.3 the same pattern is repeated with the water dimer constrained configurations collapsing to a charge difference of 0 and hydrogen sulfide dimer constraint value with charge difference of -4. The number of calculated electrons on C, N_C, approached reasonable values for constrained configurations in the homogeneous cases except for constraint value 1 for hydrogen sulfide with an N_C of 10 electrons instead of the target electrons. Then looking at the Lagrange multiplier, when considering the standard deviation of the Lagrange multiplier of the constraint values -1 and 1 of both homogeneous dimers, the Lagrange multiplier did overlap between constraint value -1 and 1 of their associated dimer.

Second, we consider the heterogeneous cases of the tetrafluoroethylene-ethylene dimer and the water-hydrogen sulfide dimer. In comparison to the homogeneous case, C and U of a heterogeneous dimer should be asymmetric, meaning E(C) $\neq$ E(U) therefore E(C^-U^+) $\neq$ E(C^+U^-). Based upon this, when comparing the energy of the constrained configurations energies to the reference in Figures 3.5, tetrafluoroethylene-ethylene dimer has distinctive constrained configurations for constraint values 1, 0, and -1 matching the predictable behavior of a heterogeneous dimer but the water-hydrogen sulfide dimer does not. This trend is repeated in Figure 3.6 with distinct charge differences between C and U for constrained configurations of the tetrafluoroethylene-ethylene dimer, but the water-hydrogen sulfide dimer's constrained configurations collapse to the reference ground state charge difference of 0. However, when looking at Table 3.2 the N_C of constrained configurations of both tetrafluoroethylene-ethylene dimer and water-hydrogen sulfide dimer are reasonable to their associated charge localized configuration. Also, the V^I of constraint value 1 and -1 were expected to differ in magnitude due to their asymmetry and this was true for both the tetrafluoroethylene-ethylene dimer and the water-hydrogen sulfide dimer.

Base upon how SCC-CDFTB performed when computing these homogeneous and heterogeneous cases, an SCC-CDFTB computation works best if charge densities between C and U of the reference ground state are asymmetric. If we look at all four dimers, the regions where

the constraint configuration is distinguishable and doesn't collapse to a reference ground state energy are at separation distances where the reference ground state charge difference between C and U is non-zero. There is an exception: the hydrogen sulfide dimer constrained configuration with a constraint value equal to 1. However, we used the same input file options and geometry for both the reference ground state and this constraint value 1 case of the hydrogen sulfide dimer. This leaves only the application of the constraint's treatment of this constrained configuration of the hydrogen sulfide dimer. This observation indicates that instead of the molecular system initially having an asymmetric charge density, the constraint value of 1 was applied twice to the constraint region. This explains both the N_C being equal to 10 electrons instead of the target 9 electrons, and the charge difference between C and U is -4. It also explains how we could perform the computation without an initial asymmetric charge density because the first application of the constraint breaks the symmetry of charge density and the second application exacerbates that difference. So, whether the asymmetric charge density is applied externally by the input file or internally within the DFTB+ framework for an SCC-CDFTB computation to produce reasonable representations of constrained configurations, the reference must have asymmetric charge density.

4.1 Reaching Convergence

During the initial stages of the SCC-CDFTB computations, the biggest impediment to the process was a lack of convergence. The bulk of computations would fail to converge. Due to this, we made several modifications to the input file and decisions in the DFTB+ framework to increase the convergence of the SCC-CDFTB method. This section discusses our mixer choice and the different ways we perturbed the molecular system to improve the convergence.

4.1.1 Mixer Choice

There are four mixers that were considered for the SCC-CDFTB Broyden,[34] Anderson,[35] DIIS,[36] and Simple mixers. These mixers are were tested by tracking the energy and number of calculated electrons, N_C, within two scenarios. The first scenario is by first setting the projection matrix entirely equal to one, then setting a row and column to 0. This action removes an atomic orbital contribution from the projection matrix. We continued this process until all atomic orbitals contributions are removed from the projection matrix. The second scenario is having CDFTB computations utilize Lagrange multipliers equal to values 1 to 0 in increments of 0.1. We tested this approach on a constrained configuration of a water dimer with a constraint value of 1. The priority of these tests was to see which mixer improves convergence the most, but also how much it assists SCC-CDFTB, which is measured by the mixer's impact on N_C,

Mixer:	Anderson	DIIS	Broyden	Simple
ProjM Convergence Number	8	10	8	9
ProjM $\langle N_C \rangle$	9.658854968	8.27644201	3.773844406	5.835467724
ProjM σ_{N_C}	7.106476496	7.227838685	4.593348214	7.314040571
Lagr Convergence Number	11	11	11	10
Lagr $\langle N_C \rangle$	8.995063535	8.999160852	8.994207137	8.993381392
Lagr σ_{N_C}	0.018194678	0.001242433	0.018495604	0.020330509

Table 4.1 Statistical analysis of the Lagrange multiplier test and Projection matrix test on four different mixers and the impact it had on the number of converged computations, average computed electrons on the constraint N_C, and standard deviation of N_C.

Based upon Table 4.1, DIIS was the chosen mixer moving forward due to it having both the greatest number of converged SCC-CDFTB computations and producing the most accurate N_C for this constrained configuration. Despite the application of the DIIS mixer to SCC-CDFTB computations for either the homogeneous or heterogeneous dimers there was

still very poor convergence. This led us to delve into the DFTB+ option of modifying the parameters of the DIIS mixer, and one of these parameters is the number of generations considered for mixing. Looking at Figure 4.1, we can see that when comparing the three generations versus six generations, there was increased convergence with three generations of mixing. There are other options utilized in Figure 4.1 which are electronic temperature (T) and initial charges (I). These options were tested on a constrained configuration on a water dimer with a constraint value of 1 across separations between 0.0 and 7.0 angstroms.

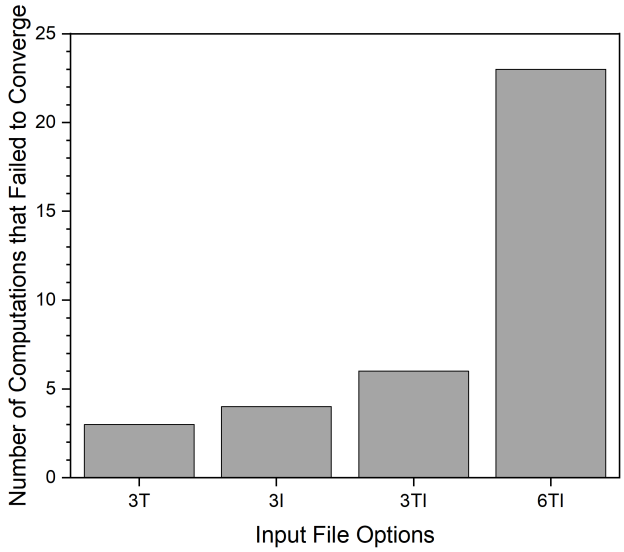

Figure 4.1 Convergence of a 3 DIIS generation with a electronic temperature option on (T), 3 DIIS generations with a initial charges turned on (I), 3 DIIS generations with options I and T turned on, and 6 DIIS generations with options I and T turned on.

4.1.2 Effective Electronic Perturbation

Despite the massive improvements to convergence made by lowering the number of generations in the DIIS mixer, several SCC-CDFTB computations failed to converge. We started the process of creating an asymmetric charge density on the reference ground state by perturbing the electron density of the reference ground state. We did this first by using a DFTB+ option to apply an electronic temperature (T) of 300K, and by doing so, DFTB+ will distribute the single particles based upon a Fermi distribution. We made this choice with

the mindset that if we perturb the molecular system, it will ease the formation of constrained configurations by partially populating virtual orbitals that are intrinsically more diffuse and potentially relevant to charge transfer. This idea is also the reasoning behind establishing the initial charges (I). Establishing the charges beforehand to be closer to or proportional to the partial charges of a constrained configuration will hopefully set the path for the SCC-CDFTB computation. We can see the effect of these two options in Figure 4.1 where option 3T had only three failed SCC-CDFTB computations, 3I had four computations fail, and with both options T and I turned on had a total of six computations fail to converge. Despite both having a positive effect on convergence, they did not work well together. Therefore we decided upon using only the electronic temperature option moving forward. This work developed the convergence strategy utilizing a DIIS mixer and a electronic temperature option that was used in the Results chapter.

Chapter Five

Conclusion

All of the work behind the implementation process of applying a charge constraint in conjunction with a configuration interaction into the DFTB framework of DFTB+ and the evaluation of this CDFTB method has been presented. The objective of this work was not only the successful implementation of this CDFTB-CI method but also the capability of this CDFTB-CI method to compute the electronic coupling of an electron transfer. The result was a SCC-DFTB computation with an applied constraint capable of building constrained configurations from references with an asymmetric charge density but no configuration interaction. A configuration interaction can not be performed unless two SCC-CDFTB computations are performed back to back, constructing two constrained configurations. Therefore, without the capabilities to properly reset all related variables between the two SCC-DFTB computations, we cannot yet perform the configuration interaction. Fortunately, all the variables in the equation used for the configuration interaction are built during the construction of the constrained configurations produced by SCC-CDFTB. We can then use the quality of the constrained configurations to gain insight into the possible quality of the electronic coupling. The analysis of the SCC-CDFTB computations demonstrated that reference ground states with a asymmetric charge densities can produce reasonable constrained configurations, but for reference ground states with symmetric charge densities, building constrained configurations is far more difficult. Also, there are promising practices that can be used to improve

these SCC-CDFTB computations. The first being the DIIS mixer with a low number of generations of mixing had a significant positive effect on the convergence of these SCC-CDFTB computations. As well as the application of an electronic temperature at 300K or the defining the initial charges also had a positive effect on convergence.

Possible future efforts should focus initially on internal and external methods that perturb the reference ground state. The internal method is by working directly in the DFTB+ framework, and the external method is by testing other DFTB+ options for the input file. However, it is essential to note that any perturbation performed on the reference ground state must be reflected in the construction of all constrained configurations because they are built from a similar reference ground state. Following this potential project, would be executing two SCC-CDFTB computations to run back to back, followed by a configuration interaction. An evaluation of the quality of the electronic couplings produced by CDFTB-CI can be performed.

REFERENCES

(1) Warshel, A. *J. Phys. Chem.* **1982**, *86*, 2218–2224.

(2) Newton, M. D. *Chem. Rev.* **1991**, *91*, 767–792.

(3) Kubař, T.; Elstner, M. *Phys. Chem. Chem. Phys.* **2013**, *15*, 5794.

(4) Troisi, A.; Nitzan, A.; Ratner, M. A. *J. Phys. Chem.* **2003**, *119*, 5782–5788.

(5) Kubas, A.; Gajdos, F.; Heck, A.; Oberhofer, H.; Elstner, M.; Blumberger, J. *Phys. Chem. Chem. Phys.* **2015**, *17*, 14342–14354.

(6) Surakhot, Y.; Laszlo, V.; Chitpakdee, C.; Promarak, V.; Sudyoadsuk, T.; Kungwan, N.; Kowalczyk, T.; Irle, S.; Jungsuttiwong, S. *J. Comput. Chem.* **2017**, *38*, 901–909.

(7) Kanlayakan, N.; Kungwan, N.; Kowalcyzk, T. Computational Analysis of Charge Carrier Mobility in MIDA-linked Covalent Organic Frameworks (in preparation)., 2019.

(8) Medina, D. D.; Sick, T.; Bein, T. *Adv. Energy Mater.* **2017**, *7*, 170387.

(9) Band, Y. B.; Avishai, Y., *Quantum Mechanics: with Applications to Nanotechnology and Information Science*; AP: 2013; Chapter Density Functional Theory, pp 871–890.

(10) Elstner, M.; Seifert, G. *Phil. Trans. R. Soc. A* **2014**, *372*, 20120483.

(11) Koskinen, P.; Mäkinen, V. *Comput. Mater.* **2009**, *47*, 237–253.

(12) Aradi, B.; Hourahine, B.; Frauenheim, T. *Phys. Chem. A* **2007**, *111*, 5678–5684.

(13) Voorhis, T. V.; Wu, Q. *Phys. Rev. A* **2005**, *11*.

(14) Rapacioli, M.; Spiegelman, F.; Scemama, A.; Mirtschink, A. *J. Chem. Theory Comput.* **2011**, *7*, 44–55.

(15) Hohenberg, P.; Kohn, W. *Phys. Rev.* **1964**, *136*, B864–B871.

(16) Bagayoko, D. *AIP Adv.* **2014**, *4*, 127104.

(17) Garrigue; Louis *J. Stat. Phys.* **2019**, *177*, 415–437.

(18) Sousa, S. F.; Fernandes, P. A.; Ramos, M. J. *J. Phys. Chem. A* **2007**, *111*, 10439–10452.

(19) Parr, R. G.; Yang, W., *Density-Functional Theory of Atoms and Molecules*; OUP: 1994; Chapter Density Functional Theory, pp 51–53.

(20) Kohn, W.; Sham, L. J. *Phys. Rev.* **1965**, *140*, A1133–A1138.

(21) Seifert, G.; Porezag, D.; Frauenheim, T. *Int. J. Quantum Chem.* **1996**, *58*, 185–192.

(22) Oliveira, A. F.; Seifert, G.; Heine, T.; Duarte, H. A. **2009**, *20*, 1193–1205.

(23) Argaman, N.; Makov, G. *Am. J. Phys.* **2000**, *68*, 69–79.

(24) Wu, Q.; Yang, W. *J. Chem. Phys.* **2003**, *118*, 2498.

(25) Foulkes, W. M. C.; Haydock, R. *Phys. Rev. B* **1989**, *39*, 12520–12536.

(26) Gaus, M.; Cui, Q.; Elstner, M. *J. Chem. Theory Comput.* **2011**, *7*, 931–948.

(27) Otte, N.; Scholten, M.; Thiel, W. *J. Phys. Chem. A* **2007**, *111*, 5751–5755.

(28) Elstner, M. *J. Phys. Chem. A* **2007**, *111*, 5614–5621.

(29) Elstner, M.; Porezag, D.; Jungnickel, G.; Elsner, J.; Haugk, M.; Frauenheim, T.; Suhai, S.; Seifert, G. *Phys. Rev. B* **1998**, *58*, 7260–7268.

(30) Porezag, D.; Frauenheim, T.; Köhler, T.; Seifert, G.; Kaschner, R. *Phys. Rev. B* **1995**, *51*, 12947–12957.

(31) Valiev, M. et al. *Comput. Phys. Commun.* **2010**, *181*, 1477–1489.

(32) Marcus D Hanwell Donald E Curtis, D. C.L.T.V.E. Z.; Hutchison, G. R. *J. Cheminformatics* **2012**, *4*, 17.

(33) Shao, Y et al. *Phys. Rev. A* **2005**, *72*, 024502.

(34) Johnson, D. D. *Phys. Rev. B* **1988**, *38*, 12807–12813.

(35) Eyert, V. *J. Comput. Phys.* **1996**, *124*, 271–285.

(36) Pauly, P. *Chem. Phys. Lett.* **1980**, *73*, 393–398.